

Quantum ellipsometry using correlated-photon beams

Kimani C. Toussaint, Jr.,¹ Giovanni Di Giuseppe,¹ Kenneth J. Bycenski,¹ Alexander V. Sergienko,^{1,2,*} Bahaa E. A. Saleh,¹ and Malvin C. Teich^{1,2}

¹*Department of Electrical & Computer Engineering, Quantum Imaging Laboratory, Boston University, 8 Saint Mary's Street, Boston, Massachusetts 02215, USA*

²*Department of Physics, Quantum Imaging Laboratory, Boston University, 8 Saint Mary's Street, Boston, Massachusetts 02215, USA*

(Received 9 March 2004; published 9 August 2004)

We report ellipsometric measurements made on semiconductor samples using photon-correlated beams produced by the process of spontaneous parametric down-conversion. Such a source yields higher accuracy than its quantum-limited conventional counterpart. We also show that our approach has the added advantage of not requiring an external reference sample for calibration.

DOI: 10.1103/PhysRevA.70.023801

PACS number(s): 42.50.Lc, 42.25.Ja, 42.50.Dv

I. BACKGROUND

Since all optical measurements are limited by quantum noise, which dominates at low light levels, there has been a strong interest in developing nonclassical optical sources with sub-Poisson photon statistics that offer sub-shot-noise accuracy. One implementation that has been considered for metrology applications is based on the use of two optical beams, each with Poisson-distributed photons, but also with a fully correlated joint photon counting distribution. Such correlated-photon beams have been generated, for example, by spontaneous parametric down-conversion (SPDC) in a nonlinear optical crystal, and used for applications including quantum cryptography [1], teleportation [2], and metrology [3,4]. If one of the beams is reflected from, or transmitted through, a sample, then measurement of the photon coincidence rate, together with the mean photon counts in each beam, yield estimates of the sample reflectance/transmittance with accuracy greater than the conventional measurement using a single beam [5–9]. In this paper, we consider the use of photon-correlated beams in ellipsometry.

Ellipsometry [10–15] is a technique in which the polarization of light is used to determine the optical properties of a material (sample) and infer information such as the thickness of a thin film. The sample is characterized by two parameters $\psi = \arctan|\tilde{r}_2/\tilde{r}_1|$ and $\Delta = \arg(\tilde{r}_2/\tilde{r}_1)$ where \tilde{r}_1 and \tilde{r}_2 are the sample's eigenpolarization complex reflection coefficients [11]. In a conventional ellipsometer, these parameters are extracted by manipulation of the polarization state of the incident or the reflected/transmitted light and measurement of the optical intensities or the photon counting rates. Clearly, such measurements are limited by shot noise, particularly at low light intensities or when using ellipsometers employing a nulling technique. The use of photon-correlated beams in ellipsometry has been previously reported and referred to as “quantum ellipsometry” [16,17]. It was shown that this technique alleviates the need for calibration using an external reference sample.

In this paper, we report experimental quantum ellipsometric measurements made on standard optical samples. We also

estimate the accuracy advantage attained by the use of quantum relative to conventional ellipsometry. Section II of the paper reviews the theory of correlated-photon ellipsometry, a form of quantum ellipsometry. Although correlated-photon pairs may be generated by a variety of means, correlated-photon ellipsometry in this paper refers to the use of photon pairs generated by SPDC. In Sec. III we present experimental results obtained from two semiconductor samples demonstrating how the technique operates. Finally, in Sec. IV we discuss the role that quantum noise plays in obtaining accurate measurements for both conventional and non-classical sources of light.

II. CORRELATED-PHOTON ELLIPSOMETRY

It has previously been shown that twin photons generated by SPDC can be used in a coincidence-detection scheme to achieve the absolute calibration of an optical detector [18–20]. In this section, we demonstrate how the addition of the polarization degree of freedom allows accurate ellipsometric measurements to be obtained.

In correlated-photon ellipsometry, a form of quantum ellipsometry, a laser (pump) beam illuminates a nonlinear optical crystal (NLC). A portion of the pump photons are converted into pairs, traditionally known as signal and idler, which conserve energy (frequency matching) and momentum (phase matching) [21,22]. For our purposes, we choose the SPDC to be in a configuration known as “type-I noncollinear”. Type I refers to the fact that the signal and idler photons have parallel polarizations; the term noncollinear indicates that the signal and idler photons are emitted in two different directions.

The light at the output of the NLC is in a polarization-product state and is described by

$$|\Psi\rangle = |HH\rangle, \quad (1)$$

where H represents horizontal polarization. In one arm of the setup, as shown in Fig. 1, the idler beam first passes through linear polarizer P followed by an $SU(2)$ element [$SU(2)_1$], which can be represented by the action of a polarization rotator sandwiched between two wave retarders, and can perform any general unitary operation. Then, the idler beam

*Electronic address: alexserg@bu.edu

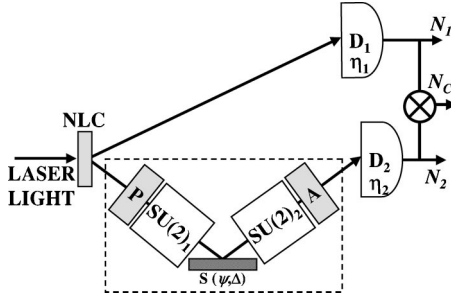


FIG. 1. Correlated-photon ellipsometry. $SU(2)_{1,2}$ represents the allowed polarization devices used, P a linear polarizer, A a linear polarization analyzer, and $D_{1,2}$ single-photon detectors with efficiencies $\eta_{1,2}$. The sample S is characterized by the ellipsometric parameters ψ and Δ , as defined in the text.

reflects off the sample of interest [$S(\psi, \Delta)$] before it encounters a second $SU(2)$ element [$SU(2)_2$], followed by a linear polarization analyzer A and then a single-photon photodetector D_2 . The 2×2 Jones matrix representation for such an operation is given by

$$\mathbf{T}_{SU(2)_j} = \begin{pmatrix} \cos \theta_j e^{i(\phi_j + \alpha_j)} & -\sin \theta_j e^{i(\phi_j - \alpha_j)} \\ \sin \theta_j e^{-i(\phi_j - \alpha_j)} & \cos \theta_j e^{-i(\phi_j + \alpha_j)} \end{pmatrix}, \quad (2)$$

where $\theta_j (j=1, 2)$ represents the angle of the axis of a polarization rotator with respect to the horizontal direction, while ϕ_j and α_j represent the retardation imparted by wave retarders. Please note that, upon cascading the Jones matrices for the overall optical system, ϕ_2 and α_1 become common terms that vanish at detection. It is also important to mention that beam splitters are not included in the apparatus because they are additional sources of noise at low light levels. In the other arm, the signal beam is simply detected by single-photon photodetector D_1 . Generally, narrowband interference filters are placed in front of each detector in order to select the degenerate-frequency photons. The detectors, two avalanche photodiodes operating in the Geiger mode, are part of a circuit that records the coincidence rate of photon pairs.

It can be shown that for the state described in Eq. (1), the obtained coincidence rate, N_c , at the detectors is given by [17]

$$N_c(t; \psi, \Delta, \phi_1, \alpha_2, \theta_1, \theta_2) = CI_{\text{in}}(t) \eta_1 \eta_2 |\tilde{r}_1|^2 |\tan \psi e^{i(\Delta + \phi_1 + \alpha_2)} \times \cos \theta_1 \cos \theta_2 - \sin \theta_1 \sin \theta_2|^2, \quad (3)$$

where $I_{\text{in}}(t)$ is the pump intensity and is assumed to vary at a time scale slower than the coincidence counting time, the constant of proportionality C includes the efficiency of down-conversion, and η_1 and η_2 are the quantum efficiencies of D_1 and D_2 , respectively. If the pump intensity were not time varying, one could determine the ellipsometric parameters of the sample in a straightforward fashion simply by choosing different angle settings for θ_1 , for example, while scanning θ_2 . However, this measurement protocol fails since the pump intensity does depend on time. To address this problem, we have developed a procedure that employs an auxiliary measurement, the singles rate. This rate has been

defined to be proportional to the intensity of the pump and the quantum efficiency of the detector [3]. Let us define the singles rate for the sample-free optical path to be

$$N_1 = CI_{\text{in}}(t) \eta_1, \quad (4)$$

while the singles rate for the optical path with the sample present is given by

$$N_2(\psi, \Delta, \phi_1, \alpha_2, \theta_1, \theta_2) = CI_{\text{in}}(t) \eta_2 |\tilde{r}_1|^2 |\tan \psi e^{i(\Delta + \phi_1 + \alpha_2)} \times \cos \theta_1 \cos \theta_2 - \sin \theta_1 \sin \theta_2|^2. \quad (5)$$

By dividing the expression in Eq. (3) by that in Eq. (4), we obtain a normalized coincidence rate N_n given by

$$\begin{aligned} N_n(\psi, \Delta, \phi_1, \alpha_2, \theta_1, \theta_2) &= \frac{N_c}{N_1} \\ &= \eta_2 |\tilde{r}_1|^2 |\tan \psi e^{i(\Delta + \phi_1 + \alpha_2)} \cos \theta_1 \cos \theta_2 \\ &\quad - \sin \theta_1 \sin \theta_2|^2. \end{aligned} \quad (6)$$

To determine the ellipsometric parameters of the sample, we can choose the following strategy. For θ_1 set to 90° and θ_2 scanned,

$$N_n(\psi, \Delta, \phi_1, \alpha_2, 90, \theta_2) = \eta_2 |\tilde{r}_1|^2 \sin^2 \theta_2 \equiv N_{90}. \quad (7)$$

Similarly, for θ_1 set to 0° and θ_2 scanned,

$$N_n(\psi, \Delta, \phi_1, \alpha_2, 0, \theta_2) = \eta_2 |\tilde{r}_1|^2 \tan^2 \psi \cos^2 \theta_2 \equiv N_0. \quad (8)$$

From these equations it is clear that ψ is

$$\psi = \arctan \sqrt{\left(\frac{N_0}{N_{90}}\right) \cot^2 \theta_2}. \quad (9)$$

To determine Δ we can set ϕ_1 to -90° , α_2 to 0° , θ_1 to $\pm 45^\circ$, and scan θ_2 . The resulting expression is

$$\begin{aligned} N_n(\psi, \Delta, 90, 0, \pm 45, \theta_2) &= \left[\frac{N_{90}}{2} + \frac{N_0}{2} \pm \eta_2 \tan \psi \right. \\ &\quad \left. \times \cos(\Delta - 90) \cos \theta_2 \sin \theta_2 \right]. \end{aligned} \quad (10)$$

In general, the value chosen for ϕ_1 depends on the sample. For example, for a bulk dielectric material the value of Δ will be close to either 0° or 180° , depending on whether the angle of incidence of the light is above or below the Brewster angle [12]. In this region, the cosine function is not sensitive to small changes. A 90° phase shift is therefore added to increase this sensitivity.

We see from the aforementioned protocol that the ellipsometric parameters are determined without the necessity of calibration by an external reference sample, independently of whether the pump intensity might vary in time, and without knowledge of the values of the quantum efficiencies of the detectors. Furthermore, since down-conversion allows for a statistical copy of a beam to be created without a beam splitter, it is possible to eliminate noise sources inherent in the system without introducing errors. This is advantageous for

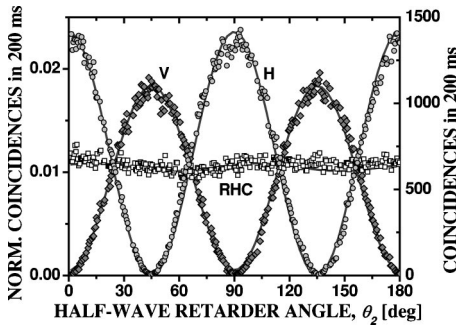


FIG. 2. Coincidence interference patterns obtained from a Si sample. The labels H , V , and RHC correspond to a horizontal, vertical, and right-hand-circular input polarization state of the light. Each sinusoidal pattern represents the sample's response to the particular polarization state. θ_2 is the angle of the axis of the half-wave retarder placed after the sample, with respect to the horizontal direction. The solid sinusoidal curves correspond to the expected theoretical fit obtained from Eq. (6).

low light levels, as we will show later, and is a feature unique to the quantum nature of correlated-photon ellipsometry.

III. EXPERIMENTAL RESULTS

In this section, we present experimental results showing how correlated-photon ellipsometry can be used to obtain values of ψ and Δ without calibration by an external reference sample. These values are comparable to those obtained from traditional ellipsometers.

The actual experimental setup used to perform our measurements differs little from the one shown in Fig. 1. Our source was a 351-nm cw Ar^+ laser. The NLC was β -barium borate, typically referred to as BBO, of 1 mm thickness. The $\text{SU}(2)$ element following the sample was a half-wave retarder while the one preceding it was chosen to be a cascade of half-wave and quarter-wave retarders. Interference filters centered at 702 nm with 10-nm bandwidths were placed before each detector. We define the angles θ_1 and θ_2 to be the angles of the axes of the half-wave retarders before and after the sample, respectively, with respect to the horizontal direction.

Using the procedures specified in Eqs. (7)–(10), ellipsometric data were obtained for a bulk single-crystal Si sample oriented such that the angle of incidence was 28° . The results are represented by the interferometric curves in Fig. 2. The labels H , V , and RHC correspond to a horizontal, vertical, and right-hand-circular input polarization state of the light. Each sinusoidal pattern represents the sample's response to the particular polarization state. Because the amplitude for the V curve is smaller than that for the H curve, we see that the Si sample preferentially absorbs vertical polarization over horizontal. As we know from Eq. (9), these H and V curves provide us with our value for ψ . The third interference pattern in Fig. 2 represents the sample's response to right-hand-circular polarization. Since Si is a bulk dielectric, we expect that the phase shift Δ imparted upon reflection should be close to either 0° or 180° .

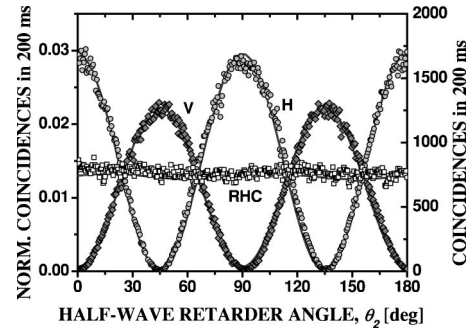


FIG. 3. Coincidence interference patterns obtained from a GaAs sample. The labels H , V , and RHC correspond to a horizontal, vertical, and right-hand-circular input polarization state of the light. Each sinusoidal pattern represents the sample's response to the particular polarization state. θ_2 is the angle of the axis of the half-wave retarder placed after the sample, with respect to the horizontal direction. The solid sinusoidal curves correspond to the expected theoretical fit obtained from Eq. (6).

With this in mind, the experimentally determined values for ψ and Δ were compared to those obtained with calculations carried out using the appropriate Sellmeier dispersion formula [23,24]. Using our correlated-photon ellipsometer, we determined that $\psi = (41.70 \pm 0.02)^\circ$ and $\Delta = (178.4 \pm 0.3)^\circ$. According to the theoretical model, the expected values are $\psi = 41.2^\circ$ and $\Delta = 179.8^\circ$. We carried out a second experiment using a bulk GaAs sample. Under the same experimental conditions, GaAs has similar optical properties to Si. In this case we obtained experimental values of $\psi = (41.20 \pm 0.03)^\circ$ and $\Delta = (178.6 \pm 0.2)^\circ$. The expected theoretical values are $\psi = 41.2^\circ$ and $\Delta = 179.7^\circ$. The results are shown in Fig. 3.

Using correlated-photon ellipsometry, the experimentally determined values of ψ and Δ are shown to be in good agreement with the expected theoretical values. The small discrepancy from the expected values is attributed to possible errors arising from angular misalignment of the optical components and of the angle of incidence. These types of problems have been shown to be common sources of errors in ellipsometry, and the standard techniques developed to reduce these errors can be similarly applied here [11].

IV. STATISTICAL ACCURACY

In this section, we compare the accuracy of the measured ellipsometric parameters obtained using a conventional coherent laser beam to that using correlated-photon beams. For this purpose, we regard the polarization system in the dashed box in Fig. 1 as an effective reflector (or beam splitter) with intensity reflectance R that is a function of ψ , Δ , and the polarization settings (of course, no NLC in the conventional method). We derive expressions for the signal-to-noise ratio (SNR) of R for systems that employ a conventional laser beam as well as for systems that use correlated-photon beams (CPB). We subsequently determine the relative error in ψ and Δ for both cases. Comparison shows that the correlated-photon beam implementation yields higher accuracy under certain conditions.

We begin with the conventional (conv) measurement. The detector, with quantum efficiency η , counts the total number of photoevents N_1 and N_2 in time duration T , in the absence and in the presence of the reflector, respectively. The simplest estimate of the reflectance

$$R = \frac{\langle N_2 \rangle}{\langle N_1 \rangle} \quad (11)$$

is the ratio

$$\hat{R}_{\text{conv}} = \frac{N_2}{N_1}. \quad (12)$$

Since N_1 and N_2 are random, the estimate \hat{R}_{conv} is also random, and its statistics determine the measurement error.

To determine the mean and variance, and hence the signal-to-noise ratio of \hat{R}_{conv} , it is convenient to think of the number of counts N_1 (or N_2) as a sum of M statistically independent and identically distributed Bernoulli random variables representing the photon registrations in M short time intervals, each of duration T/M [25]. The photon rate is assumed to be sufficiently small such that the probability of more than one photoevent in a time T/M is negligible. We define p to be the mean number of photons in this time interval. It follows that N_1 and N_2 have binomial distributions, with means $\langle N_1 \rangle = \eta M p$ and $\langle N_2 \rangle = \langle N_1 \rangle R$, and variances

$$\text{var}(N_1) = \langle N_1 \rangle \left(1 - \frac{\langle N_1 \rangle}{M} \right) \quad (13)$$

and

$$\text{var}(N_2) = \langle N_2 \rangle \left(1 - \frac{\langle N_2 \rangle}{M} \right), \quad (14)$$

respectively. The finite reflectance of the sample and the finite quantum efficiency of the detector do not change the binomial statistics of N_1 and N_2 [26], since the underlying Bernoulli distribution is invariant to random deletion [9].

It is not easy to determine the statistics of the ratio given in Eq. (12). For this purpose, we assume that the deviations of N_1 and N_2 from their respective means are small, so that

$$\begin{aligned} \hat{R}_{\text{conv}} &= \frac{\langle N_2 \rangle}{\langle N_1 \rangle} \left(1 + \frac{N_2 - \langle N_2 \rangle}{\langle N_2 \rangle} \right) \left(1 + \frac{N_1 - \langle N_1 \rangle}{\langle N_1 \rangle} \right)^{-1} \\ &\approx R \left(1 + \frac{N_2}{\langle N_2 \rangle} - \frac{N_1}{\langle N_1 \rangle} \right), \end{aligned} \quad (15)$$

where R is the ratio of the means. Since N_1 and N_2 are independent,

$$\text{var}(\hat{R}_{\text{conv}}) = R^2 \left(\frac{\text{var}(N_2)}{\langle N_2 \rangle^2} + \frac{\text{var}(N_1)}{\langle N_1 \rangle^2} \right). \quad (16)$$

The SNR is therefore

$$(\text{SNR}_{\text{conv}}) = \frac{R^2}{\text{var}(\hat{R}_{\text{conv}})} = \frac{M \langle N_2 \rangle}{[M(1+R) - 2\langle N_2 \rangle]}. \quad (17)$$

We now move on to the SNR for the CPB system (see Fig. 1). The random variables N_1 and N_2 are defined in the same way as in the conventional case, but because of the common origin of each beam, N_1 and N_2 are correlated. In addition, the number of coincidences is a binomial random variable N_c , with mean

$$\langle N_c \rangle = \eta_2 \langle N_1 \rangle R \quad (18)$$

and variance

$$\text{var}(N_c) = \langle N_c \rangle \left(1 - \frac{\langle N_c \rangle}{M} \right). \quad (19)$$

In this case, we use the ratio

$$\hat{R}_{\text{CPB}} = N_c / N_1 \quad (20)$$

to estimate the product $\eta_2 R$. To determine the mean and variance of \hat{R}_{CPB} we approximate Eq. (20) as

$$\begin{aligned} \hat{R}_{\text{CPB}} &= \frac{\langle N_c \rangle}{\langle N_1 \rangle} \left(1 + \frac{N_c - \langle N_c \rangle}{\langle N_c \rangle} \right) \left(1 + \frac{N_1 - \langle N_1 \rangle}{\langle N_1 \rangle} \right)^{-1} \\ &\approx \eta_2 R \left(1 + \frac{N_c}{\langle N_c \rangle} - \frac{N_1}{\langle N_1 \rangle} \right), \end{aligned} \quad (21)$$

where we have assumed that the variations of N_1 and N_c are small compared to their respective means. This has permitted us to convert a ratio N_c/N_1 to a difference $N_c - N_1$, which is far more tractable. The mean value of \hat{R}_{CPB} is $\eta_2 R$. The variance is given by

$$\text{var}(\hat{R}_{\text{CPB}}) = (\eta_2 R)^2 \left[\frac{\text{var}(N_c)}{\langle N_c \rangle^2} + \frac{\text{var}(N_1)}{\langle N_1 \rangle^2} - 2 \frac{\text{cov}(N_c, N_1)}{\langle N_c \rangle \langle N_1 \rangle} \right], \quad (22)$$

where the variances in N_1 and N_c are given in Eq. (13) and Eq. (19), respectively.

The last term in Eq. (22) is a result of the correlated nature of N_c and N_1 . By tracing the origins of these two random variables back to a common Bernoulli random variable that results from the random arrival of a photon pair in a time slot, and two independent Bernoulli deletion processes, it can be shown that

$$\text{cov}(N_c, N_1) = \langle N_c \rangle \left(1 - \frac{\langle N_1 \rangle}{M} \right). \quad (23)$$

Therefore, we determine the SNR to be

$$(\text{SNR}_{\text{CPB}}) = \frac{(\eta_2 R)^2}{\text{var}(\hat{R}_{\text{CPB}})} = \frac{\langle N_c \rangle \langle N_1 \rangle}{\langle N_1 \rangle - \langle N_c \rangle}. \quad (24)$$

We see from Eq. (24) that if we have ‘‘perfect’’ correlation $\langle N_c \rangle$ equals $\langle N_1 \rangle$ and the SNR for the CPB system is infinite. The finite quantum efficiencies of the detectors employed, as well as the overall reflectance of the system, serve to reduce this correlation and therefore the SNR.

Figure 4 shows the SNR for both the conventional and CPB cases. For the purposes of comparison, we have assumed that the mean number of photons in the interval T/M , which must be small, is approximately $p=0.001$ and M ,

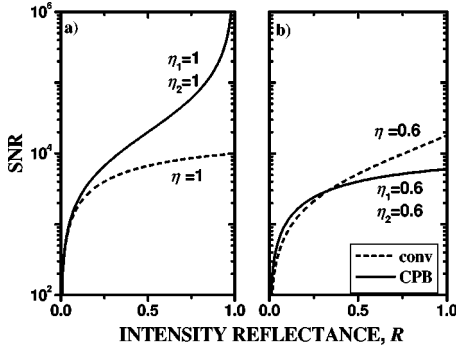


FIG. 4. Comparison of the signal-to-noise ratio, as a function of the effective intensity reflectance R , for correlated-photon beams (solid curves) and the conventional system (dashed curves) for two values of the quantum efficiency: (a) $\eta = \eta_1 = \eta_2 = 1$; (b) $\eta = \eta_1 = \eta_2 = 0.6$.

which must be large, is chosen to be $M = 2 \times 10^7$. We observe from Fig. 4(a) that, when the quantum efficiencies of the detectors are unity, the SNR of the CPB system is higher than that of the conventional system for all values of R . We also see that the enhancement factor is greater for higher values of R . As shown in Fig. 4(b), for lower quantum efficiencies, the enhancement factor is reduced below that shown in Fig. 4(a). We also see that the CPB system does not perform as well as the conventional system when R dips below a certain threshold. The value of this threshold depends on the quantum efficiencies of the detectors. This is because the coincidence rate is sensitive to the quantum efficiency of two detectors rather than just a single detector as in the single beam case, i.e., the coincidence rate decreases faster than the count rate in the single channel.

Now that we have determined the error in estimating the reflectance/transmittance R of the ellipsometric system, we proceed to determine the corresponding error in estimating the ellipsometric parameters ψ and Δ . For both the conventional and the CPB techniques, R is related to these parameters [referring to Eqs. (5) and (6), respectively, with $\phi_1 = \alpha_2 = 0$] by

$$R(\psi, \Delta, \theta_1, \theta_2) = C |\tan \psi e^{i\Delta} \cos \theta_1 \cos \theta_2 - \sin \theta_1 \sin \theta_2|^2, \quad (25)$$

where θ_1 and θ_2 are the angles of the ellipsometer, and C is a constant of proportionality appropriate to the CPB or conventional system.

Three measurements of R at three sets of angles are sufficient to estimate the three unknown parameters ψ , Δ , and C . A convenient set of angles leads to the three equations

$$R_1 \equiv R(\psi, \Delta, 90, 90) = C, \quad (26)$$

$$R_2 \equiv R(\psi, \Delta, 0, 0) = C \tan^2 \psi, \quad (27)$$

and

$$R_3 \equiv R(\psi, \Delta, 45, 45) = \frac{C}{4} |\tan \psi e^{i\Delta} - 1|^2, \quad (28)$$

which may be solved to obtain the following expressions for ψ , Δ

$$\psi = \arctan \sqrt{\frac{R_2}{R_1}} \quad (29)$$

and

$$\Delta = \arccos \left(\frac{4R_3 - R_1 - R_2}{2\sqrt{R_1 R_2}} \right). \quad (30)$$

Since only statistical estimates of the three reflectances \hat{R}_1 , \hat{R}_2 , and \hat{R}_3 are available, the corresponding estimates of the ellipsometric parameters based on Eq. (29) and Eq. (30) are

$$\hat{\psi} = \arctan \sqrt{\frac{\hat{R}_2}{\hat{R}_1}} \quad (31)$$

and

$$\hat{\Delta} = \arccos \left(\frac{4\hat{R}_3 - \hat{R}_1 - \hat{R}_2}{2\sqrt{\hat{R}_1 \hat{R}_2}} \right). \quad (32)$$

Since the estimators \hat{R}_1 , \hat{R}_2 , and \hat{R}_3 are statistically independent, we may use error propagation techniques [27] to write the variances of the estimated ellipsometric parameters as

$$\text{var}(\hat{\psi}) = \left(\frac{\partial \psi}{\partial R_2} \right)^2 \text{var}(\hat{R}_2) + \left(\frac{\partial \psi}{\partial R_1} \right)^2 \text{var}(\hat{R}_1) \quad (33)$$

and

$$\begin{aligned} \text{var}(\hat{\Delta}) &= \left(\frac{\partial \Delta}{\partial R_3} \right)^2 \text{var}(\hat{R}_3) + \left(\frac{\partial \Delta}{\partial R_2} \right)^2 \text{var}(\hat{R}_2) \\ &+ \left(\frac{\partial \Delta}{\partial R_1} \right)^2 \text{var}(\hat{R}_1). \end{aligned} \quad (34)$$

We are now in a position to determine the relative errors in estimating the ellipsometric parameters for either the CPB or conventional system by using Eq. (29) and Eq. (30) to determine the derivatives in Eq. (33) and Eq. (34), and the expression in Eq. (16) or Eq. (22) to determine the variances of \hat{R}_1 , \hat{R}_2 , and \hat{R}_3 for both techniques.

Figure 5 shows the relative error in $\hat{\psi}$, $e_\psi = \text{var}(\hat{\psi})/\psi^2$, for both the CPB and conventional systems for two different quantum efficiencies. We observe from Fig. 5(a) that the error is larger for the conventional case for all values of ψ when the quantum efficiencies of all detectors used are unity, with the largest difference being an order of magnitude improvement in e_ψ for the CPB system over the conventional system. A similar effect is seen in Fig. 6(a) where the relative error in $\hat{\Delta}$, $e_\Delta = \text{var}(\hat{\Delta})/\Delta^2$, is compared for the two systems when $\psi = 45^\circ$. Again, the error is larger for the conventional system for all values of Δ when the detector quantum efficiencies are unity. Choosing different values of ψ yields similar curves for e_Δ .

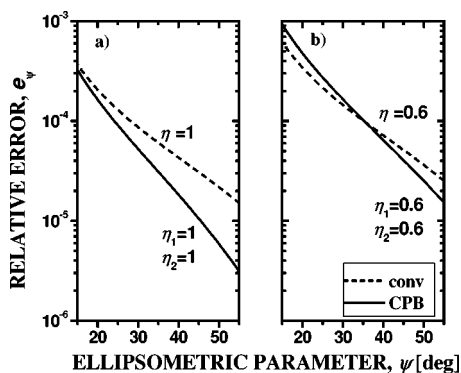


FIG. 5. The relative error e_ψ in the ellipsometric parameter ψ for correlated-photon beams (solid curves) and the conventional system (dashed curves) for two values of the quantum efficiency: (a) $\eta = \eta_1 = \eta_2 = 1$; (b) $\eta = \eta_1 = \eta_2 = 0.6$.

We also see from Figs. 5(b) and 6(b) that, for quantum efficiencies that are appreciably less than unity, e_ψ and e_Δ for the CPB case approach those of the conventional case. The reason for this was considered earlier in the context of deriving the SNR. Specifically, the coincidence rate, which is used only in the CPB system, is sensitive to the square of the quantum efficiency rather than just to the quantum efficiency of a single detector, as in the conventional system.

V. CONCLUSION

Conventional ellipsometric measurements are limited in their accuracy because of unavoidable noise fluctuations that dominate in the low-light regime. Quantum ellipsometry can mitigate this limitation by using correlated-photon pairs created by the SPDC process, in conjunction with a coincidence-counting detection scheme. It has the added advantage that it does not require calibration by an external reference sample.

An experimental demonstration of correlated-photon ellipsometry has been carried out for two bulk semiconductor

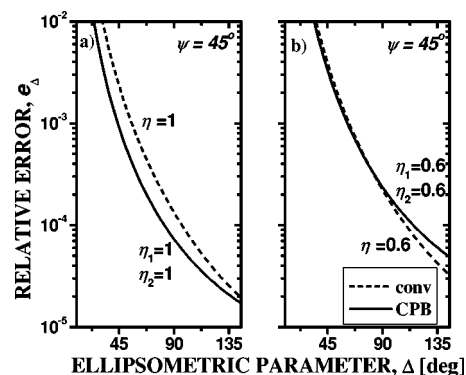


FIG. 6. The relative error e_Δ in the ellipsometric parameter Δ for $\psi = 45^\circ$ for correlated-photon beams (solid curves) and the conventional system (dashed curves) for two values of the quantum efficiency: (a) $\eta = \eta_1 = \eta_2 = 1$; (b) $\eta = \eta_1 = \eta_2 = 0.6$.

samples. We obtained experimental values that are in good agreement with the expected theoretical values. These measurements were obtained without calibration by an external reference sample.

We presented a model for determining the signal-to-noise ratio of the measured ellipsometric parameters. We showed that systems employing correlated-photon beams have a larger SNR than those using a conventional source when the quantum efficiencies of the detectors are high.

In our scheme, we have exploited only the property of photon number correlation and not polarization entanglement. What role does polarization entanglement play in ellipsometric measurements? We are currently exploring this question and will report on this elsewhere.

ACKNOWLEDGMENTS

This work was supported by the Gates Millennium Scholars Program, the National Science Foundation, and the Center for Subsurface Sensing and Imaging Systems (CenSSIS), a NSF engineering research center.

-
- [1] A. K. Ekert, J. G. Rarity, P. R. Tapster, and G. M. Palma, *Phys. Rev. Lett.* **69**, 1293 (1992).
- [2] C. H. Bennett, G. Brassard, C. Crepeau, R. Jozsa, A. Peres, and W. K. Wootters, *Phys. Rev. Lett.* **70**, 1895 (1993).
- [3] D. N. Klyshko, *Sov. J. Quantum Electron.* **7**, 591 (1977).
- [4] D. Branning, A. L. Migdall, and A. V. Sergienko, *Phys. Rev. A* **62**, 063808 (2000).
- [5] B. E. A. Saleh, *Photoelectron Statistics* (Springer, New York, 1978).
- [6] J. G. Rarity, P. R. Tapster, and E. Jakeman, *Opt. Commun.* **62**, 201 (1987).
- [7] M. C. Teich and B. E. A. Saleh, in *Progress in Optics* (North-Holland, Amsterdam, 1988), pp. 1–104.
- [8] P. R. Tapster, J. G. Rarity, and J. S. Satchell, *Phys. Rev. A* **37**, 2963 (1988).
- [9] M. M. Hayat, A. Joobeur, and B. E. A. Saleh, *J. Opt. Soc. Am. A* **16**, 348 (1999).
- [10] P. Drude, *Ann. Physik Chemie* **39**, 481 (1890).
- [11] R. M. A. Azzam and N. M. Bashara, *Ellipsometry and Polarized Light* (North-Holland, Amsterdam, 1977).
- [12] H. G. Tompkins and W. A. McGahan, *Spectroscopic Ellipsometry and Reflectometry* (Wiley, New York, 1999).
- [13] A. Rothen, *Rev. Sci. Instrum.* **16**, 26 (1945).
- [14] A. B. Winterbottom, *Trans. Faraday Soc.* **42**, 487 (1946).
- [15] M. Mansuripur, *Opt. Photonics News* **11**(4), 52 (2000).
- [16] A. F. Abouraddy, K. C. Toussaint, Jr., A. V. Sergienko, B. E. A. Saleh, and M. C. Teich, *Opt. Lett.* **26**, 1717 (2001).
- [17] A. F. Abouraddy, K. C. Toussaint, Jr., A. V. Sergienko, B. E. A. Saleh, and M. C. Teich, *J. Opt. Soc. Am. B* **19**, 656 (2002).
- [18] D. N. Klyshko, *Kvantovaya Elektron. (Moscow)* **7**, 1932 (1980) [*Sov. J. Quantum Electron.* **10**, 1112 (1980)].
- [19] A. Migdall, R. Datla, A. V. Sergienko, and Y. H. Shih,

- Metrologia **32**, 479 (1995).
- [20] A. Migdall, S. Castelletto, I. P. Degiovanni, and M. L. Rastello, *Appl. Opt.* **41**, 2914 (2002).
- [21] D. N. Klyshko, *Photons and Nonlinear Optics* (Nauka, Moscow, 1980, Gordon and Breach, New York, 1988), Chaps. 1 and 6.
- [22] B. E. A. Saleh and M. C. Teich, *Fundamentals of Photonics* (Wiley, New York, 1991).
- [23] *Handbook of Optical Constants of Solids*, edited by E. D. Palik (Academic Press, New York, 1985).
- [24] *Handbook of Optical Constants of Solids III*, edited by E. D. Palik (Academic Press, New York, 1995).
- [25] B. E. A. Saleh and M. C. Teich, *Fundamentals of Photonics* (Wiley, New York, 1991b), Chap. 11.
- [26] M. C. Teich and B. E. A. Saleh, *Opt. Lett.* **7**, 365 (1982).
- [27] J. Mandel, *The Statistical Analysis of Experimental Data* (Interscience Publishers, New York, 1964).